New Journal of Physics
The open access journal at the forefront of physics

Deutsche Physikalische Gesellschaft DPG IOP Institute of Physics

PAPER • OPEN ACCESS

EPR-based ghost imaging using a single-photon-sensitive camera

To cite this article: Reuben S Aspden *et al* 2013 *New J. Phys.* **15** 073032

New Journal of Physics
The open access journal for physics

EPR-based ghost imaging using a single-photon-sensitive camera

Reuben S Aspden[1,4], Daniel S Tasca[1,4], Robert W Boyd[2,3] and Miles J Padgett[1]

[1] SUPA, School of Physics and Astronomy, University of Glasgow, Glasgow G12 8QQ, UK
[2] Institute of Optics, University of Rochester, Rochester, NY 14627, USA
[3] Department of Physics, University of Ottawa, Ottawa, ON K1N 6N5, Canada
E-mail: r.aspden.1@research.gla.ac.uk and daniel.tasca@glasgow.ac.uk

New Journal of Physics **15** (2013) 073032 (11pp)
Received 14 May 2013
Published 17 July 2013
Online at http://www.njp.org/
doi:10.1088/1367-2630/15/7/073032

Abstract. Correlated photon imaging, popularly known as ghost imaging, is a technique whereby an image is formed from light that has never interacted with the object. In ghost imaging experiments, two correlated light fields are produced. One of these fields illuminates the object, and the other field is measured by a spatially resolving detector. In the quantum regime, these correlated light fields are produced by entangled photons created by spontaneous parametric down-conversion. To date, all correlated photon ghost imaging experiments have scanned a single-pixel detector through the field of view to obtain spatial information. However, scanning leads to poor sampling efficiency, which scales inversely with the number of pixels, N, in the image. In this work, we overcome this limitation by using a time-gated camera to record the single-photon events across the full scene. We obtain high-contrast images, 90%, in either the image plane or the far field of the photon pair source, taking advantage of the Einstein–Podolsky–Rosen-like correlations in position and momentum of the photon pairs. Our images contain a large number of modes, >500, creating opportunities in low-light-level imaging and in quantum information processing.

[4] Authors to whom any correspondence should be addressed.

Contents

1. Introduction

In a ghost imaging system, the object and the imaging detector are illuminated by two correlated, spatially separated light beams, and the ghost image is obtained from intensity correlations between the two light fields. These optical correlations can occur in either the quantum or classical regime [1]. Ghost imaging was first demonstrated in 1995 by Pittman *et al* [2], who used correlated photon pairs generated by spontaneous parametric down-conversion (SPDC). They used one of the down-converted fields to illuminate an aperture, and the transmission through it was detected by a non-imaging, single-pixel detector, termed the bucket detector. An image of the aperture was obtained from the coincidence counts between this bucket detector and a scanning single-pixel detector in the other beam. Bennink *et al* [3] demonstrated ghost imaging using a classical light source, and Ferri *et al* [4] have since shown that ghost imaging using classical light sources can match some results thought to be obtainable only when using entangled light. However, these classical systems cannot produce high-resolution, background-free images derived from both position and momentum correlations within the same source [5]. Since ghost imaging was first proposed there has been a large body of published work, using both thermal [3–10] and quantum entangled light [5, 11–15].

All previous realizations of ghost imaging using SPDC photons have relied on scanning a detector to measure the spatial distribution of the optical field. This scanning necessarily limits the detection efficiency of such an imaging system to a maximum of $1/N$, where N is the number of scanned pixels. In this work, we overcome this limitation and present a practical ghost imaging system at the single-photon level by using a time-gated, intensified CCD (ICCD) camera. Our advance inherently increases the detection efficiency of a ghost imaging system proportionally to the number of pixels, N, in the image. The use of a camera allows us to capture high-visibility ghost images across the full field of view. The object is placed in one arm (object arm) of the SPDC, the transmission through which is detected by a large-area bucket detector. The ICCD is placed in the other arm (camera arm) and is triggered using the output from the bucket detector, each frame recording the position where the single photon was detected. We compensate for the electronic delay associated with the triggering of the camera by means of a folded, image preserving delay line (DL) as illustrated in figure 1.

Our system was designed with interchangeable lenses that allow us to utilize either the intensity correlations of the photon pairs in the image plane of the down-conversion source

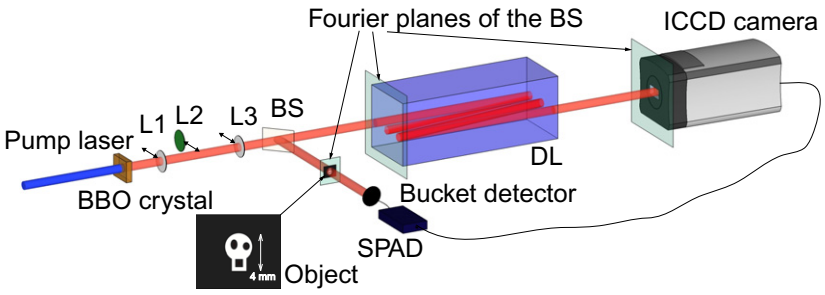

Figure 1. Schematic diagram of the experimental setup. Collinear down-converted photon pairs at 710 nm are generated by pumping a β-barium borate (BBO) crystal with a UV laser at 355 nm. L_1 and L_3 are 50 mm focal length lenses used to produce an image of the down-conversion source onto the beam splitter (BS). L_2 is a 100 mm focal length lens used to Fourier transform the exit facet of the down-conversion source onto the BS. A 300 mm focal length lens (not shown) is used after the BS in each path to Fourier transform the down-converted fields at the BS onto the planes of the object in one arm and onto the input plane of an image preserving DL in the other arm. The image preserving DL consists of seven imaging systems with a total length of 22 m. Our object (inset) is a transmissive mask with the shape of a skull printed on acetate.

or their anti-correlation in the far field. This capability of using image-plane or far-field correlations allows us to explore the Einstein–Podolsky–Rosen (EPR)-like correlations in the transverse position or momentum of the photon pairs [16]. In our system, the correlations are not those between the camera and the bucket detector, rather the bucket detector measures the photons whose spatial state is defined by the object; hence the correlations we observe are between the object and the image.

The major advantage of full field-of-view detection, compared to a scanning system, is the dramatic increase in efficiency in the measurement of high-dimensional spatial entanglement. Recent work has demonstrated the potential of the multi-pixel detection of spatial entanglement [17–22] and, for multiple photons, quantum imaging [23]. In our work, the combination of multi-mode coincidence detection and single-photon sensitivity across an entire field of view suggests applications in low-light imaging systems, and quantum information protocols utilizing spatial states such as quantum key distribution [24, 25], information processing [26] and teleportation [27].

2. Experimental methods

A schematic diagram of our experimental setup is shown in figure 1. Our down-conversion source consists of a 3 mm long β-barium borate (BBO) crystal cut for type-I phase matching and pumped with a horizontally polarized, high-repetition-rate laser at 355 nm. The pump laser is spatially filtered and re-collimated to a diameter of approximately 1.2 mm (FWHM) at the crystal. The BBO crystal is oriented to provide near-collinear, frequency-degenerate, down-converted photons centred at 710 nm over a 10 nm bandwidth, determined by high-transmission interference filters. We use a pellicle BS to split the photon pairs into the object and camera arms.

As we use a collinear type-I SPDC source, only 50% of the photon pairs are split into different paths at the BS. The photons used to probe the object are detected with a bucket detector, with a field of view that extends over the whole scene. This bucket detector registers whether the photons have passed through the object while recording no direct image information. Our bucket detector consists of a lens that couples the photons into a multi-mode fibre connected to a single-photon avalanche diode (SPAD).

Our ghost image is obtained by using the bucket detector to trigger a single-photon acquisition by the ICCD (Andor iStar, Gen 2 image intensifier, WR photo-cathode); we subsequently sum these camera images over many trigger events. The pump power was adjusted to approximately 2 mW, giving a trigger rate from the bucket detector of approximately 15 kHz for the image-plane configuration and 10 kHz for the far-field configuration. This was chosen to be compatible with the maximum response rate of the ICCD while minimizing the possibility of overlapping trigger pulses. The ICCD was air cooled to $-15\,^{\circ}$C and operated in direct gate mode, where the transistor–transistor logic (TTL) pulse from the SPAD triggers the intensifier of the camera directly, giving a gate width equal to the length of the trigger pulse.

To obtain in-focus images, the ICCD camera and the object must be located in planes where the down-converted photons exhibit strong intensity correlations [28]. We chose two configurations that satisfy this condition. In the first configuration, both the object and the ICCD are placed in image planes of the BBO crystal, where the positions of the photons are correlated. In the second configuration, the object and the ICCD are placed in the far field of the BBO crystal, where the positions of the photons are anti-correlated, arising from their momentum anti-correlation. We choose between these two configurations through use of an interchangeable lens system located between the BBO crystal and the BS, as indicated in figure 1. The ability to show strong correlations in complementary variables, such as in momentum and position, is the hallmark of entanglement and is not possible with a classical source [16, 29].

In order to allow for the electronic delay associated with the bucket detector and the trigger mechanism in the ICCD camera ($\approx$70 ns), the photon in the camera arm has to be delayed before it arrives at the ICCD. Our DL consists of consecutive imaging systems with unit magnification (see figure A.1). There are a total of seven such imaging systems in the DL, four of which are formed with 1000 mm focal length lenses and three with 500 mm focal length lenses, giving a total distance of propagation of 22 m. Using the aforementioned interchangeable lens system, the two configurations set a relationship between the crystal and object/camera planes that are characterized by either an imaging system with magnification $M = 3$ or a Fourier system with effective focal length $f_e = 300$ mm (see appendix A).

3. Image acquisition

Figure 2 shows a set of ghost images taken in both the position correlated and momentum anti-correlated configurations for several different values of the delay of the triggering pulse (adjusted by changing the length of the cable between the SPAD and the ICCD). As the timing of the triggering pulse is changed relative to the time of arrival of the correlated photon on the ICCD, the coincidence is lost and therefore no image is recorded. Figures 2(a) and (b) show the optimum ghost images in the two configurations, both with a contrast in excess of 90%.

All images were obtained by summing 1800 accumulations of 2 s duration. This accumulation time was chosen in order to ensure that each individual accumulation was spatially sparse, and therefore photon counting could be applied. In this regime it is desirable to have a

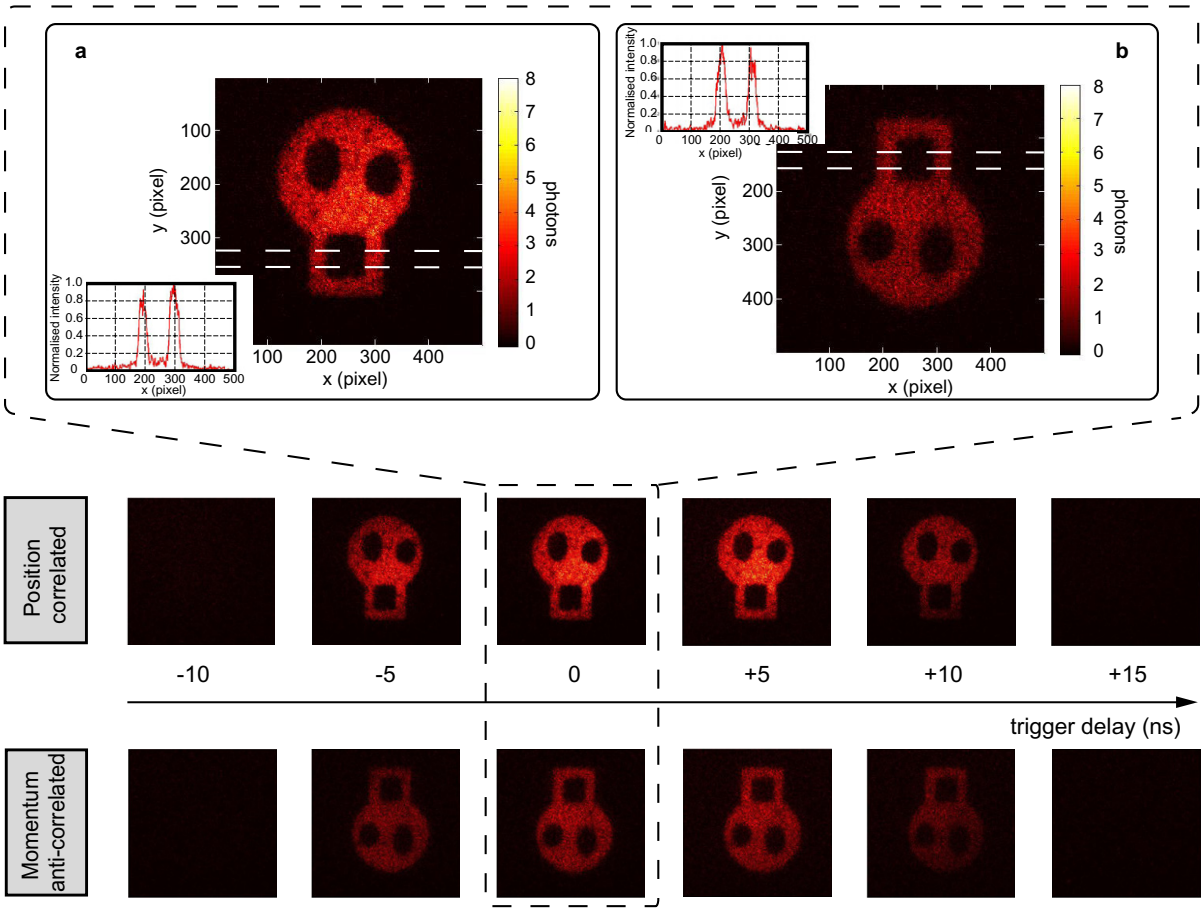

Figure 2. Ghost images and trigger delay timing. Ghost images obtained in the position correlated and momentum anti-correlated configurations as a function of the trigger delay, with a total integration time of 1 h per image. The delay is scanned in increments of 5 ns, which corresponds to adding/removing 1 m of cable. The images shown in (a) and (b) are enlarged versions of the images obtained with optimum delay time, for which the total number of photo-events was 124 310 and 74 021, respectively. The insets show cross-sections of the images averaged over the 30 rows indicated by the dashed lines.

mean number of photons per mode of much less than one, as the threshold does not distinguish between one and many photons. The resolution of the ICCD is set not by the pixel size but rather by the resolution of the intensifier. Incident photons on the intensifier are converted into photoelectrons, which are multiplied. These photoelectrons fluoresce on a phosphor screen and the photons are detected at the CCD chip. This process sets the resolution and is manifested as a blooming of the photo-events across several pixels on the CCD chip [30]. To compensate for this limited resolution, we apply a spatial filter where each event smaller than two pixels in extent is attributed to read-out noise on the chip and is subtracted from the image. Using this photon counting methodology, the average number of detected photons per frame was approximately 70 in the position correlated configuration and 40 in the momentum anti-correlated configuration. The intensity scale of the displayed images is the summed number of detected photons per mode. Importantly, no background subtraction was applied to any of the images.

In the position correlated configuration the image is upright, figure 2(a). In the momentum anti-correlated configuration the resulting image is inverted, figure 2(b). As the optical magnification in each arm is the same, the sizes of both images on the ICCD match the actual size of the object. The resolution of both images is comparable and is set by a combination of the correlation length of the down-converted photons and the resolving power of our optical system (see appendix B).

The ability to obtain high-resolution, background-free images in both the position correlated and momentum anti-correlated configurations is enabled by utilization of the EPR-like correlations in the spatial variables of the down-converted photons. By analysing the bright-to-dark transitions within the images, we obtain point spread functions (PSFs) for our ghost imaging system with standard deviations given by $\sigma_{\text{pos}} = 81\,\mu$m in the position configuration and $\sigma_{\text{mom}} = 135\,\mu$m in the momentum configuration[5]. These standard deviations are indicative of the strength of the position and the momentum correlations of the photon fields in the plane of the ICCD and the object. Although not strictly equivalent to a conditional probability distribution across the whole field, they are nevertheless good measures of the strength of the intensity correlations. We estimate the standard deviations of the position, Δ_{pos}, and momentum, Δ_{mom}, correlations at the SPDC source from σ_{pos} and σ_{mom} and the parameters of the optical systems according to $\Delta_{\text{pos}} = \sigma_{\text{pos}}/M$ and $\Delta_{\text{mom}} = (k/f_{\text{e}})\sigma_{\text{mom}}$. We note that their variance product of $0.012\hbar^2$ is smaller than $\hbar^2/4$.

As an alternative to obtaining ghost images of the object shown in figure 1, we also recorded images using pinholes of 75 and 200 μm in diameter. Although of less complexity as an image, the ghost images of the pinholes give the detection probability of the photons in the camera arm conditioned on the measurement of the photons in the object arm within a small spatial extent as defined by the pinhole. These conditional probabilities lead more directly to a measure of the strength of the correlations as strictly required in a demonstration of EPR correlations [31]. Using these pinholes, we calculated the standard deviations of the PSFs in position and momentum to be $\Delta^x_{\text{pos}} = (49 \pm 1)\,\mu$m, $\Delta^y_{\text{pos}} = (49 \pm 3)\,\mu$m, $\Delta^x_{\text{mom}} = (128 \pm 7)\,\mu$m and $\Delta^y_{\text{mom}} = (140 \pm 8)\,\mu$m giving a variance product of $(3.8 \pm 0.1) \times 10^{-3}\hbar^2$ and $(4.5 \pm 0.2) \times 10^{-3}\hbar^2$ in the x and y directions, respectively. Slight differences between these values and those inferred from the bright-to-dark transitions of the images can be attributed to defocus from the ideal case. However, the strengths of the correlations observed in both the printed image and the pinhole are indicative of EPR correlations.

4. Information content of the images

The amount of information contained in the transverse distribution of a single photon is an important question in the context of a communication or cryptographic system [24, 32, 33]. Two practical limitations to consider when using spatial states in this way are the resolution of the measurement apparatus and the finite size of the transverse field distribution. The resolution of our optical system is set by the PSFs, as calculated above. The field distributions in the image plane and far field as detected by the camera have a standard deviation of $\Gamma_{\text{pos}} = 1.83$ mm and $\Gamma_{\text{mom}} = 3.06$ mm, respectively. As the object and the ICCD are positioned in equivalent planes, these field distributions correspond to those illuminating the object. The largest dimension of

[5] Using cross-sections of the images, we calculate the standard deviations of the PSFs from the width corresponding to the transition from 90 to 10% of the maximum intensity. This width is equal to 2.56σ.

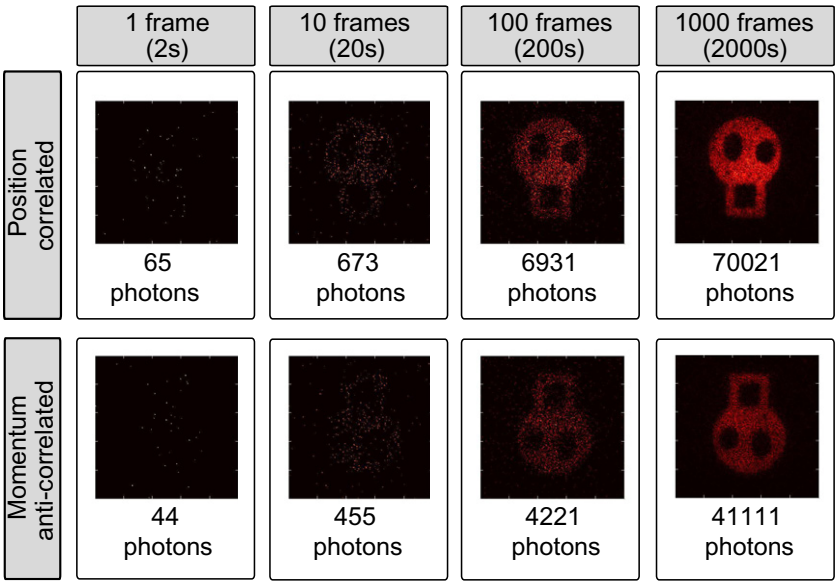

Figure 3. Photon counting and heralding efficiency. Images obtained in position correlated and momentum anti-correlated configurations for an increasing number of acquired frames, along with the corresponding number of detected photons. Each frame is the result of a thresholding procedure of the recorded intensity distributions over an accumulation time of 2 s.

the object is 4 mm (see figure 1), so it is enclosed within a region smaller than 2.2Γ of the illumination beam in both configurations. Considering an information encoding based on binned transverse position states of the single photons, our optical system can distinguish up to $(\Gamma/\sigma)^2$ orthogonal states. Using the PSF and beam widths quoted above, we calculate that our optical system can resolve approximately 500 modes in both configurations. This corresponds to up to 9 bits of information per detected photon. Figure 3 shows a set of images obtained by summing an increasing number of frames. As discussed above, photon counting was performed by using intensity and spatial thresholding techniques. This gave a heralding efficiency of $\eta = 0.2\%$, which was calculated as the ratio between the average number of detected photons at the camera and the triggering rate. This heralding efficiency could be increased by changing the threshold procedures applied, but this would come at the cost of increased dark count rates and reduced visibility.

5. Discussion

We have experimentally demonstrated a practical ghost imaging system at the single-photon level by utilizing a multi-pixel, time-gated, intensified camera. We recorded full-field ghost images with 90% visibility by utilizing the spatial correlations of photon pairs in position or the anti-correlations in momentum. The ability to obtain high-contrast images using either position or momentum correlations is an image-based utilization of the EPR phenomenon.

We circumvent the time delay associated with the trigger mechanism of our camera and other components by building a free-space, image preserving optical DL. The ability to take full-field images gives a potential increase in sampling efficiency that scales with the number

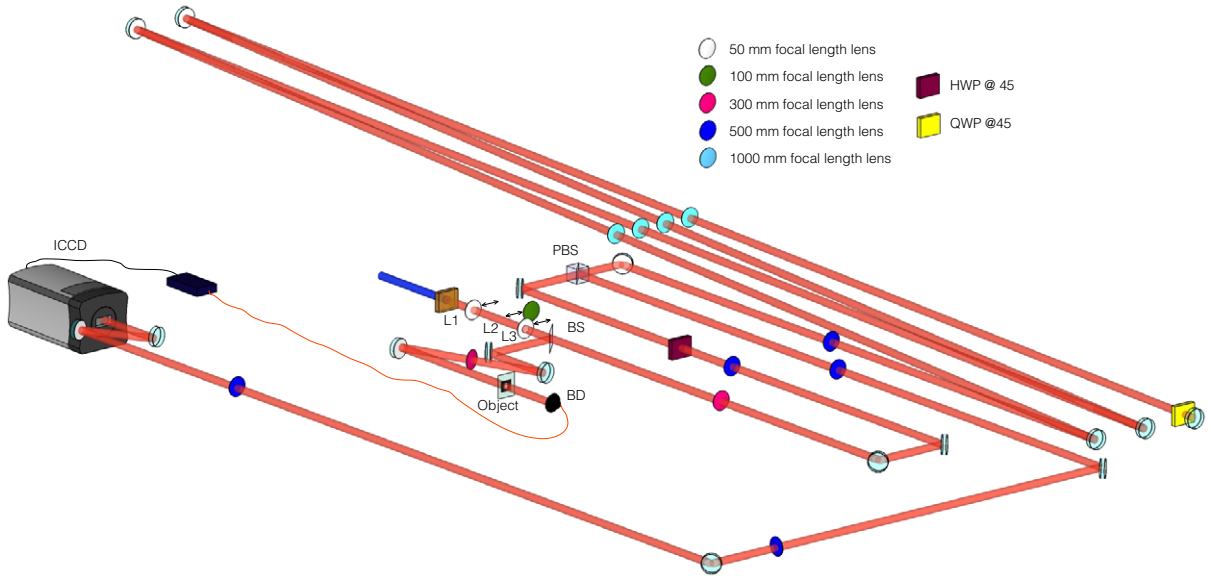

Figure A.1. Full experimental setup of our ghost imaging system.

of pixels in the image. We believe that this ghost imaging system could be useful both in imaging applications and in investigations of quantum information protocols with spatial states. Regarding imaging applications, one could envisage a non-degenerate SPDC system [34] where the object is illuminated with infrared light while the image is recorded with photons in the visible spectrum. This non-degenerate approach could be of particular interest for low-light, low-energy imaging of biological samples.

Acknowledgments

MJP thanks the Royal Society, the Wolfson Foundation and DARPA. RWB thanks the DARPA InPho programme and the Canada Excellence Research Chairs programme. We acknowledge financial support from the UK EPSRC. We thank Dr J Romero for a careful reading of the paper.

Appendix A. Image preserving delay line

We use a type-I down-conversion source with the optical axis of the BBO crystal orientated horizontally, thus generating vertically polarized down-converted photons. The polarization of the photons in the camera arm is rotated by 90° using a half-wave plate at 45°, so they are transmitted through the polarizing beam splitter (PBS). They are then imaged through the PBS to the input mirror of a telescopic imaging system with unit magnification constructed with 1 m focal length lenses. The photons propagate through this imaging system and are back-reflected along the same path, double passing through a quarter-wave plate set at 45°, thus rotating the polarization of the photons back to horizontal. They are therefore reflected when incident again on the PBS and are re-imaged on to the camera.

Appendix B. Two-photon intensity correlation

In our ghost imaging system, we make use of the intensity correlations of the photon pairs in the image plane and far field of the down-conversion source. The correlation length of the photon pairs in these planes can be estimated from the two-photon wave function and from our optical system. In the thin-crystal monochromatic and paraxial approximations, the post-selected two-photon wave function of SPDC can be written as [35, 36]

$$\Phi(\mathbf{q}_1, \mathbf{q}_2) = \mathcal{V}(\mathbf{q}_1 + \mathbf{q}_2)\gamma(\mathbf{q}_1 - \mathbf{q}_2), \tag{B.1}$$

where $\mathbf{q}_1$ ($\mathbf{q}_2$) is the transverse component of the wave vector of photon 1 (2). The function $\mathcal{V}$ is the angular spectrum of the pump beam, which is transferred to the two-photon wave function [35], and γ is the phase matching function of the SPDC. Since the angular spectrum of the pump beam $\mathcal{V}$ is much narrower than the phase matching function γ, the photon pairs exhibit anti-correlation between their transverse momenta. In our experiment, we use a fundamental Gaussian pump beam such that $\mathcal{V}$ can be approximated by a Gaussian function. The phase matching function, γ, can be described by a *sinc* function [36] and under certain conditions is approximated by a Gaussian function [36, 37].

The two-photon wave function in transverse position representation is given by the Fourier transform of equation (B.1):

$$\Psi(\boldsymbol{\rho}_1, \boldsymbol{\rho}_2) = \mathcal{W}(\boldsymbol{\rho}_1 + \boldsymbol{\rho}_2)\Gamma(\boldsymbol{\rho}_1 - \boldsymbol{\rho}_2), \tag{B.2}$$

where $\boldsymbol{\rho}_1$ and $\boldsymbol{\rho}_2$ are the transverse coordinates in the detection planes of photons 1 and 2, $\mathcal{W}$ is the transverse field distribution of the pump beam and Γ is the Fourier transform of the phase matching function. As the function Γ is much narrower than $\mathcal{W}$, the transverse positions of the photons are correlated. We define the correlation lengths of the photon pairs as the standard deviation of the two-photon detection probability distributions in the image plane and far field, which are proportional to the widths of $|\Gamma|^2$ and $|\mathcal{V}|^2$, respectively. Using the parameters of our SPDC and optical system, we use the Gaussian approximation [37] to estimate these correlation lengths as

$$\sigma_{\mathrm{IP}} \approx \frac{M}{\sqrt{2}}\sqrt{\frac{0.455L}{k_{\mathrm{p}}}} \approx 19\,\mu\mathrm{m}, \tag{B.3}$$

$$\sigma_{FF} \approx \frac{1}{\sqrt{2}}\frac{f_{\mathrm{e}}}{\sigma_{\mathrm{p}}k} \approx 33\,\mu\mathrm{m}, \tag{B.4}$$

where $L = 3\,\mathrm{mm}$ is the length of the crystal, k_{p} is the wavenumber of the pump beam, σ_{p} is the standard deviation of the amplitude of the Gaussian pump beam at the crystal and f_{e} is the effective focal length of the Fourier system. We note that these correlation lengths are both below the resolution of our optical system given by the widths $\sigma_{\mathrm{pos}} = 81\,\mu\mathrm{m}$ and $\sigma_{\mathrm{mom}} = 135\,\mu\mathrm{m}$ of the PSFs.

References

[1] Shapiro J H and Boyd R W 2012 The physics of ghost imaging *Quantum Inform. Process* **11** 949–93

[2] Pittman T B, Shih Y H, Strekalov D V and Sergienko Mg A V 1995 Optical imaging by means of two-photon quantum entanglement *Phys. Rev.* A **52** R3429–32

[3] Bennink R S, Bentley S J and Boyd R W 2002 'Two-photon' coincidence imaging with a classical source *Phys. Rev. Lett.* **89** 113601
[4] Ferri F, Magatti D, Gatti A, Bache M, Brambilla E and Lugiato L A 2005 High-resolution ghost image and ghost diffraction experiments with thermal light *Phys. Rev. Lett.* **94** 183602
[5] Bennink R S, Bentley S J, Boyd R W and Howell J C 2004 Quantum and classical coincidence imaging *Phys. Rev. Lett.* **92** 033601
[6] Gatti A, Brambilla E and Lugiato L A 2003 Entangled imaging and wave-particle duality: from the microscopic to the macroscopic realm *Phys. Rev. Lett.* **90** 133603
[7] Gatti A, Brambilla E, Bache M and Lugiato L A 2004 Correlated imaging, quantum and classical *Phys. Rev.* A **70** 013802
[8] Shapiro J H 2008 Computational ghost imaging *Phys. Rev.* A **78** 061802(R)
[9] Sun B, Welsh S S, Edgar M P, Shapiro J H and Padgett M J 2012 Normalized ghost imaging *Opt. Express* **20** 16892–901
[10] Ragy S and Adesso G 2012 Nature of light correlations in ghost imaging *Sci. Rep.* **2** 651
[11] Abouraddy A F, Saleh B E, Sergienko A V and Teich M C 2001 Role of entanglement in two-photon imaging *Phys. Rev. Lett.* **87** 123602
[12] Erkmen B I and Shapiro J H 2008 Unified theory of ghost imaging with Gaussian-state light *Phys. Rev.* A **77** 043809
[13] O'Sullivan M N, Clifford Chan K W and Boyd R W 2010 Comparison of the signal-to-noise characteristics of quantum versus thermal ghost imaging *Phys. Rev.* A **82** 053803
[14] Jack B, Leach J, Romero J, Franke-Arnold S, Ritsch-Marte M, Barnett S M and Padgett M J 2009 Holographic ghost imaging and the violation of a bell inequality *Phys. Rev. Lett.* **103** 083602
[15] Malik M, Shin H, O'Sullivan M, Zerom P and Boyd R W 2010 Quantum ghost image identification with correlated photon pairs *Phys. Rev. Lett.* **104** 163602
[16] Howell J C, Bennink R S, Bentley S J and Boyd R W 2004 Realization of the Einstein–Podolsky–Rosen paradox using momentum- and position-entangled photons from spontaneous parametric down conversion *Phys. Rev. Lett.* **92** 210403
[17] Leach J, Warburton R E, Ireland D G, Izdebski F, Barnett S M, Yao A M, Buller G S and Padgett M J 2012 Quantum correlations in position, momentum and intermediate bases for a full optical field of view *Phys. Rev.* A **85** 013827
[18] Edgar M P, Tasca D S, Izdebski F, Warburton R E, Leach J, Agnew M, Buller G S, Boyd R W and Padgett M J 2012 Imaging high-dimensional spatial entanglement with a camera *Nature Commun.* **3** 984
[19] Moreau P-A, Mougin-Sisini J, Devaux F and Lantz E 2012 Realization of the purely spatial Einstein–Podolsky–Rosen paradox in full-field images of spontaneous parametric down-conversion *Phys. Rev.* A **86** 010101
[20] Ben Dixon P, Howland G A, Schneeloch J and Howell J C 2012 Quantum mutual information capacity for high-dimensional entangled states *Phys. Rev. Lett.* **108** 143603
[21] Zhang L, Neves L, Lundeen J S and Walmsley I A 2009 A characterization of the single-photon sensitivity of an electron multiplying charge-coupled device *J. Phys. B: At. Mol. Opt.* **42** 114011
[22] Fickler R, Krenn M, Lapkiewicz R, Ramelow S and Zeilinger A 2013 Real-time imaging of quantum entanglement *Sci. Rep.* **3** 1914
[23] Brida G, Genovese M and Ruo Berchera I 2010 Experimental realization of sub-shot-noise quantum imaging *Nature Photon.* **4** 227–30
[24] Walborn S P, Lemelle D S, Almeida M P and Souto Ribeiro P H 2006 Quantum key distribution with higher-order alphabets using spatially encoded qudits *Phys. Rev. Lett.* **96** 090501
[25] Groblacher S, Jennewein T, Vaziri A, Weihs G and Zeilinger A 2006 Experimental quantum cryptography with qutrits *New J. Phys.* **8** 75
[26] Tasca D S, Gomes R M, Toscano F, Souto Ribeiro P H and Walborn S P 2011 Continuous-variable quantum computation with spatial degrees of freedom of photons *Phys. Rev.* A **83** 052325

[27] Walborn S P, Ether D S, de Matos R L Filho and Zagury N 2007 Quantum teleportation of the angular spectrum of a single-photon field *Phys. Rev.* A **76** 033801
[28] Tasca D S, Walborn S P, Souto P H Ribeiro, Toscano F and Pellat-Finet P 2009 Propagation of transverse intensity correlations of a two-photon state *Phys. Rev.* A **79** 033801
[29] Spengler C, Huber M, Brierley S, Adaktylos T and Hiesmayr B C 2012 Entanglement detection via mutually unbiased bases *Phys. Rev.* A **86** 022311
[30] Buchin M P 2011 Low-light imaging: ICCD, EMCCD and sCMOS compete in low-light imaging *Laser Focus World* **47** 7
[31] Reid M D 1989 Demonstration of the Einstein–Podolsky–Rosen paradox using non-degenerate parametric amplification *Phys. Rev.* A **40** 913–23
[32] Walborn S P, Lemelle D S, Tasca D S and Souto Ribeiro P H 2008 Schemes for quantum key distribution with higher-order alphabets using single-photon fractional fourier optics *Phys. Rev.* A **77** 062323
[33] Leach J, Bolduc E, Gauthier D J and Boyd R W 2012 Secure information capacity of photons entangled in many dimensions *Phys. Rev.* A **85** 060304
[34] Rubin M H and Shih Y 2008 Resolution of ghost imaging for non-degenerate spontaneous parametric down-conversion *Phys. Rev.* A **78** 033836
[35] Monken C H, Ribeiro P H S and Padua S 1998 Transfer of angular spectrum and image formation in spontaneous parametric down-conversion *Phys. Rev.* A **57** 3123–6
[36] Walborn S P, Monken C H, Padua S and Souto P H Ribeiro 2010 Spatial correlations in parametric down-conversion *Phys. Rep.* **495** 87–139
[37] Law C K and Eberly J H 2004 Analysis and interpretation of high transverse entanglement in optical parametric down conversion *Phys. Rev. Lett.* **92** 127903